

## High Performance Broadband Detectors from Soft X-ray to Near Infrared Range Based on Two Dimensional CrSiTe<sub>3</sub>

*Yun Li,<sup>1</sup> Jingying Liu,<sup>1</sup> Xin Su,<sup>3</sup> Qingdong Ou,<sup>1</sup> Zhichen Wan,<sup>1</sup> Yingjie Wu,<sup>1</sup> Wenzhi Yu,<sup>1</sup> Xiaozhi Bao,<sup>4</sup> Yamin Huang,<sup>5</sup> Xiaomu Wang,<sup>3</sup> Anton Tadich,<sup>6</sup> Babar Shabbir,<sup>\*1, 2</sup> Qiaoliang Bao<sup>\*1</sup>*

<sup>1</sup>Department of Materials Science and Engineering, and ARC Centre of Excellence in Future Low-Energy Electronics Technologies (FLEET), Monash University, Clayton, Victoria 3800, Australia

<sup>2</sup>Key Laboratory of Optoelectronic Devices and Systems of Ministry of Education and Guangdong Province, College of Electronic Science and Technology and College of Optoelectronics Engineering, Shenzhen University, Shenzhen University, Shenzhen 518060, P. R. China

<sup>3</sup>School of Electronic Science and Engineering Nanjing University, Nanjing, Jiangsu 210093, P. R. China

<sup>4</sup>Institute of Applied Physics and Materials Engineering (IAPME), University of Macau, Taipa, Macau, China

<sup>5</sup>State Key Laboratory of Functional Materials for Informatics, Shanghai Institute of Microsystem and Information Technology, Chinese Academy of Sciences, 865 Changning Road, Shanghai 200050, China

<sup>6</sup>Australian Synchrotron, ANSTO, 800 Blackburn Road, Clayton, Victoria 3168, Australia.

E-mail: A/Prof. Qiaoliang Bao (qiaoliang.bao@monash.edu & qiaoliang.bao@gmail.com)

and Dr. Babar Shabbir (babar.shabbir@monash.edu)

Table S1. Performance comparison of CrSiTe<sub>3</sub> based device and other detector with different materials.

Material	Measurement condition	Light Source	Sensitivity ( $\mu\text{C Gy}^{-1}\text{air cm}^{-2}$ )	Responsivity [ $\text{A W}^{-1}$ ]	EQE [%]	Detectivity [ $\text{cm Hz}^{1/2}\text{W}^{-1}$ ]	Response time [ms] (Rise)	Ref.
CrSiTe <sub>3</sub>	V <sub>DS</sub> =1 V	Synchrotron beam, 785 nm Laser, spectrograph (NIR)	463	206 (785 nm) 10 (950 nm)	32600 (785 nm) 1310(950 nm)	1.25 × 10 <sup>12</sup> (785 nm) 2.4 × 10 <sup>11</sup> (950 nm)	43 (soft X-ray) 17 (785 nm)	This work
MAPbI <sub>3</sub> film	V <sub>DS</sub> =80 V	8 KeV (CuK $\alpha$ )	25	1.25 (~650 nm)	–	–	–	1
MAPbX <sub>3</sub> films on TFT backplane	V <sub>DS</sub> =10~20 0V	Clinical angiography	11	–	–	–	<60	2
MAPbBr <sub>3</sub> SCs	-	X-tube	80	–	<30	–	0.216	3
Cs <sub>2</sub> AgBiBr <sub>6</sub> S Cs	V <sub>DS</sub> =50 V	tungsten anode X-ray tube	105	–	–	–	0.77	4
CH <sub>3</sub> NH <sub>3</sub> PbI <sub>3</sub>	V <sub>DS</sub> =3 V	300 W Xe lamp Laser	–	3.49 (365 nm) 0.0367 (780nm)	1190 (365 nm) 5.84 (780 nm)	–	<200 (365 nm) <100 (780 nm)	5
4L-MoTe <sub>2</sub>	V <sub>DS</sub> =5 V V <sub>g</sub> =-40 V	685 nm laser	–	6 (685 nm)	-	-	0.16	6
MoTe <sub>2</sub>	V <sub>DS</sub> =10 V V <sub>g</sub> =10 V	Visible to infrared laser	–	0.02	–	3.1 × 10 <sup>9</sup> (637 nm) 1.3 × 10 <sup>9</sup> (1060 nm)	1.6	7
CrGeTe <sub>3</sub>	V <sub>DS</sub> =10 mV	635/945 nm LED	–	340 (NPC, 635 nm)	-	-	1300	8
MoS <sub>2</sub> /BP	V <sub>DS</sub> =3V	532 nm Laser 1.55 $\mu\text{m}$ Laser	–	22.3 (532 nm) 153.4 (1.55 $\mu\text{m}$ )	-	3.1 × 10 <sup>11</sup> (532 nm) 2.13 × 10 <sup>9</sup> (1.55 $\mu\text{m}$ )	0.015	9
WSe <sub>2</sub>	V <sub>DS</sub> =0.2 V	370 to 1064 nm Laser	–	0.92	180	–	0.9	10
1L-2LWSe <sub>2</sub> junction	V <sub>DS</sub> =2 V, V <sub>g</sub> = -80 V	532 nm Laser	–	110 (532 nm)	256	>4 × 10 <sup>11</sup>	290	11
Monolayer MoS <sub>2</sub>	V <sub>DS</sub> = 8 V, V <sub>g</sub> = -70 V	561 nm Laser	–	880 (561 nm)	–	–	4000	12
MoSe <sub>2</sub>	V <sub>DS</sub> = 8 V, V <sub>g</sub> = -20 V	532nm Laser	–	97.1 (532 nm)	22666	–	15	13
MoO <sub>3</sub> -doped CH <sub>3</sub> NH <sub>3</sub> PbI <sub>3</sub>	V <sub>DS</sub> =1 V	450 nm Laser	–	27.3 (450 nm)	23.7	3.9 × 10 <sup>11</sup>	10	14
PdSe <sub>2</sub>	V <sub>DS</sub> =1 V V <sub>g</sub> =30 V	1064 nm Laser	–	708 (1064 nm)	82700 (1064 nm)	1.31 × 10 <sup>9</sup>	–	15
Graphene	V <sub>DS</sub> =1.5 V	sapphire laser & optical parametric amplification	–	4 (1.3 $\mu\text{m}$ ) 1.9 (2.1 $\mu\text{m}$ ) 1.1 (3.2 $\mu\text{m}$ )	–	–	–	16
BP	V <sub>DS</sub> =0.2 V	Visible laser	–	0.005 (640 nm)	–	–	1	17
BP	V <sub>DS</sub> =0.5 V	Infrared laser	–	82 (3.39 $\mu\text{m}$ )	–	–	–	18
Bi <sub>2</sub> O <sub>2</sub> Se	V <sub>DS</sub> =0.6 V	1200 nm Laser	–	65 (1200 nm)	–	3 × 10 <sup>9</sup>	10 <sup>-9</sup>	19

Table S2. Binding energy (eV) of electrons on the different shells in free Cr, Si and Te atom

Z	Element	Electron binding energies													
		K	L1	L2	L3	M1	M2	M3	M4	M5	N1	N2	N3	N4	N5
		1s	2s	2p1/2	2p3/2	3s	3p1/2	3p3/2	3d3/2	3d5/2	4s	4p1/2	4p3/2	4d3/2	4d5/2
14	Si	1839	149.7	99.82	99.42										
24	Cr	5989	696.0	583.8	574.1	74.1	42.2	42.2							
52	Te	31814	4939	4612	4341	1006	870.8	820.0	583.4	573.0	169.4	103.3	103.3	41.9	40.4

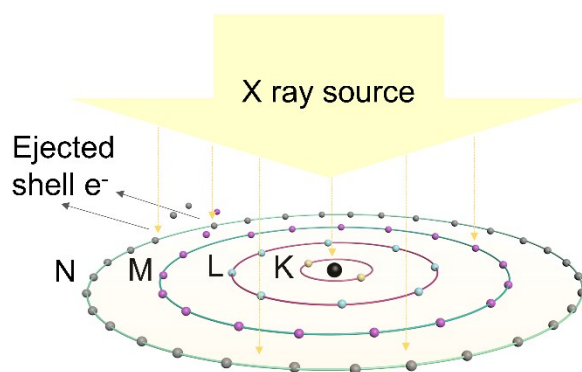


Figure S1. Schematic diagram of conversion between X-ray photon and current change taking place in CrSiTe<sub>3</sub> flake.

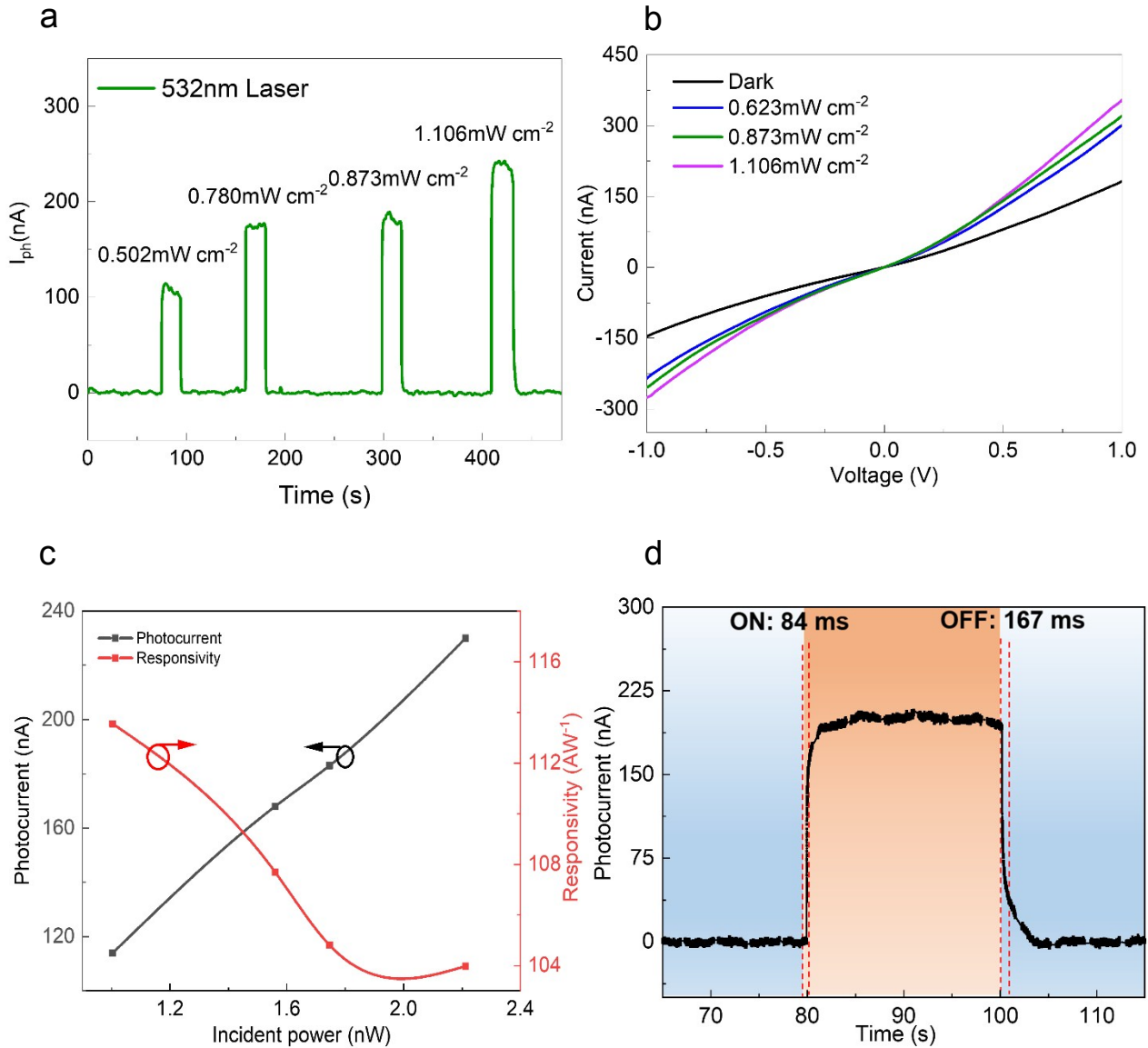


Figure S2. Device performance under 532 nm visible light. a) Time-dependent photocurrents ( $I_{\text{light}} - I_{\text{dark}}$ ) of the  $\text{CrSiTe}_3$  device. Incident light: 532 nm,  $V=1$  V. b) Photocurrents ( $I_{\text{light}} - I_{\text{dark}}$ ) of the device under different laser intensity vary with bias voltage from -1 V to 1 V. c) Photocurrent and photo-responsivity versus incident light power at 532 nm.  $V=1$  V. d) Temporal photocurrent response. The rise time ( $\approx 9.7$  ms) and the fall time ( $\approx 2.1$  s) are defined as the time for the photocurrent increase to/decreases by 70% of the ON-state current, respectively. Incident light: 532 nm laser with intensity 0.502 mW.  $V=1$  V.

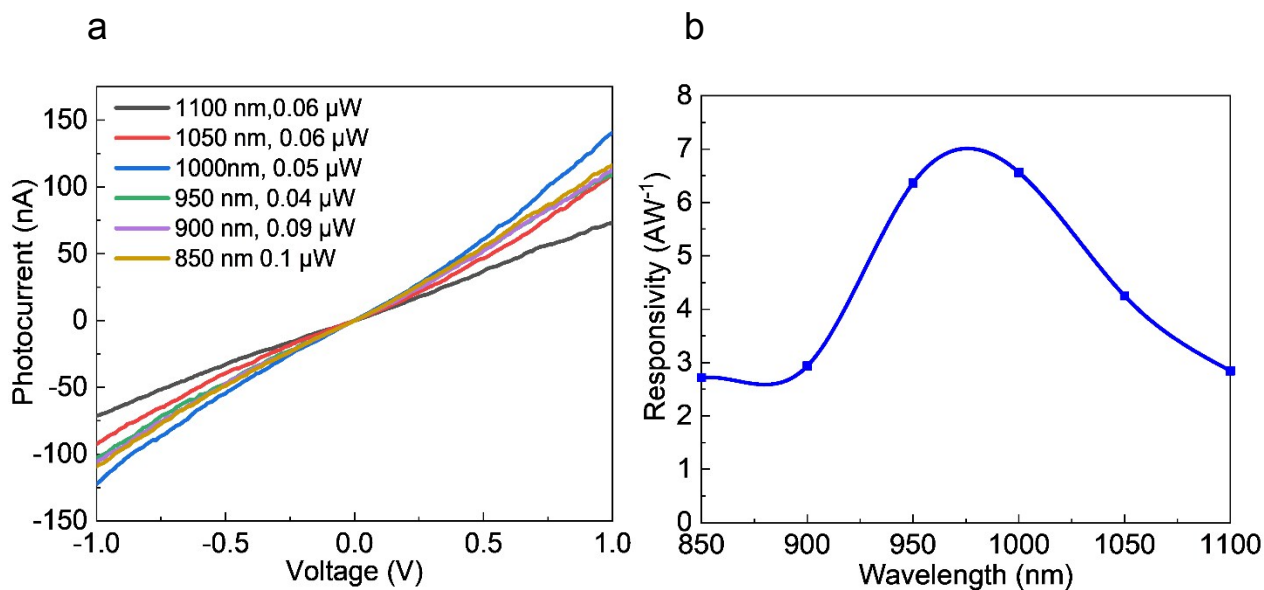


Figure S3. Device performance under near infrared light illumination. a) Photocurrents of  $\text{CrSiTe}_3$  based device under laser with different light intensity with 1 V bias voltage. Incident light: 950 nm. b) Nominalised responsivity varies with wavelength in NIR range from 850 nm to 1100 nm. The line is the fitting of dots and not represents the band gap position.

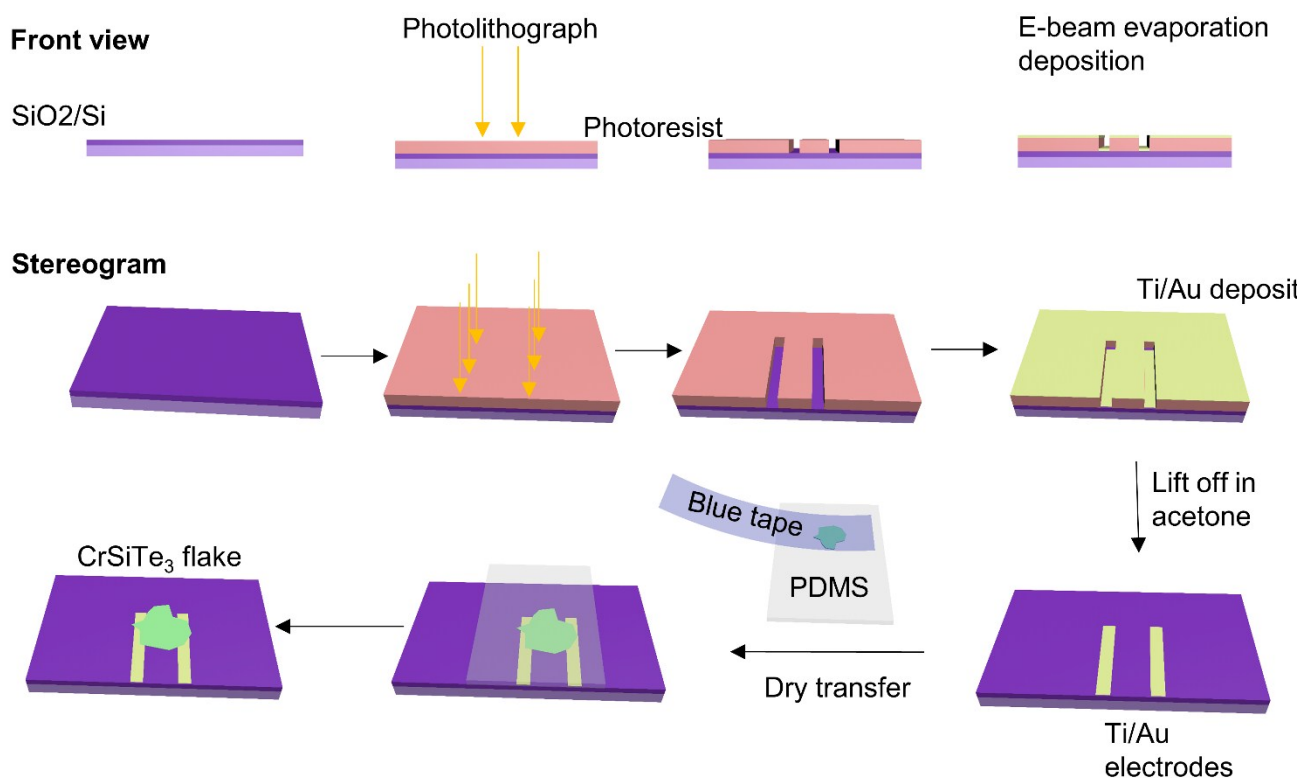


Figure S4. Schematic diagram of device fabrication process. The first line is front view of photolithography and e-beam evaporation process. The second and third line is the whole production process of  $\text{CrSiTe}_3$  device.

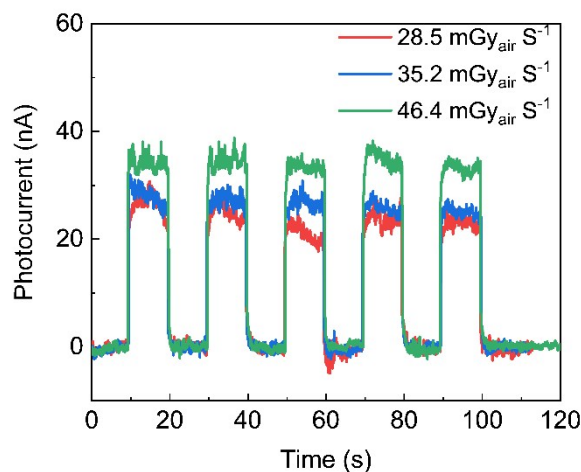


Figure S5. Device time-dependent response to X-ray on turning the X-ray source on and off under different dose rates with 1V bias voltage and X-ray energy 1200 eV.

### Supplementary notes

Supporting Note 1. Performance comparison Table.

The table list performance of photodetector based on different group of materials including perovskite, TMDc, graphene, black phosphorus and other novel vdW materials. Although there are some novel vdW materials with good performance in some aspect, such as ultra-fast response time ( $\text{Bi}_2\text{O}_2\text{Se}$ ) or much higher responsivity ( $\text{PdSe}_2$ ), they cannot perform well in every aspect. In comparison, the  $\text{CrSiTe}_3$  based photodetector has higher sensitivity ( $463 \mu\text{C Gy}^{-1}_{\text{air}} \text{cm}^{-2}$ ) than most of perovskite based photodetector ( $10 \sim 100 \mu\text{C Gy}^{-1}_{\text{air}} \text{cm}^{-2}$ ), higher responsivity ( $206 \text{ cm Hz}^{1/2} \text{W}^{-1}$ ) than most of TMDc materials based photodetector (mostly  $< 100 \text{ cm Hz}^{1/2} \text{W}^{-1}$ ), relatively fast response time (17s) and most importantly the broadband detectivity.

Supplementary Note 2. Mechanism of X-ray photons converting to secondary electrons.

In the table, the binding energies of electrons on different shells are listed for Cr, Si and Te atom. Since in this ternary compound, the electrons in outermost shell will recombined, only the electrons from secondary outer layer are listed. In our measurement, the Synchrotron beam can generate soft X-ray beam with energy from around 100 eV to 1200 eV. According to the table, the binding energy are around or less than 100 eV in the L shell of Si atom, M shell of Cr atom and N shell of Te atom. Cr and Te also have binding energy less than 1000 eV at L shell and M shell, respectively. Hence, energy of generated soft X-ray can be large than the binding energy of all these atoms in specific shell. It means that this soft X-ray beam can provide sufficient energy, which satisfies the energy requirement for electrons escape and forming secondary electrons.

Figure S1 shows a schematic diagram when X-ray beam incident totally to an atom. The total atom will under expose of Soft X-ray, when the energy of X-ray beyond the level of binding energy of electrons, these electrons will be ejected. It usually happens on N and M shell and part of L shell that includes electrons with lower binding energy.

Supplementary Note 3. Device performance under visible light 532 nm laser.

As the device performance under 785 nm has been presented in main text, the device performance under 532 nm laser was also evaluated as illustration in visible range, in figure S3. The results show an approximate linear dependence of photocurrent with incident power, to the maximum about 240 nA. The highest responsivity achieved under this wavelength can be calculated as  $114 \text{ A/W}^{-1}$ , and EQE can be calculated as 26640%. Compared with that under 785 nm laser, the maximum value of responsivity we got is lower under 532 nm, but it was measured under light with higher incident power. According to the responsivity curve results in all figures, it is obvious that the responsivity will have higher value at lower incident power. Hence, we believe the responsivity can achieve higher value under 532 nm laser, but due to the equipment limitation, we are not able to get result under lower incident power. In addition, the response time under 532 nm laser is around 84 ms, which is slower than what we got under 785 nm laser. This might be attributed to relatively larger incident power of laser that traps electrons in material.

Supplementary Note 4. Device performance under NIR range.

Figure S3 presents the device performance under NIR range light with longer wavelength from 850 nm to 1100 nm. Although the calculated responsivities are relatively lower than those under 785 nm, it's no doubt that  $\text{CrSiTe}_3$  can work in a broadband range. According to bandgap mentioned in main text, the wavelength around 1000 nm is much closer to the absorption edge, hence the responsivity at this range (smaller than  $10 \text{ A/W}$ ) is much smaller than that under 785 nm laser ( $206 \text{ A/W}$ ). Based on this big difference of responsivity, the peak appears around 1000 nm is more like fluctuation considering the facts of both light intensity and wavelength.

Supporting Note 5. Device fabrication process.

The device fabrication process including photolithography and dry transfer are present in figure S4. Firstly, one photoresist layer is spin-coated onto the surface of silicon substrate, and by using mask-free photolithography the designed shape of interspace was obtained. Following with electron beam evaporation and lift-off in acetone, electrodes consisting of Ti and Au are perfectly deposited onto the

substrate. Then CrSiTe<sub>3</sub> flake were exfoliated from bulk crystal to the transparent Polydimethylsiloxane (PDMS) sheet. By using our home-built directional transfer station, the flake can transfer directly from PDMS to the top of electrodes.

Supplementary Note 6. Stability and reproducibility of device under soft X ray measurement.

Figure S5 shows another several periods of measurement which have the similar condition with figure 2c shown in the main text but with different dose rate. The combination of these continuous tests demonstrates good stability with clear on/off photocurrent switching.

## Reference

1. S. Yakunin, M. Sytnyk, D. Kriegner, S. Shrestha, M. Richter, G. J. Matt, H. Azimi, C. J. Brabec, J. Stangl, M. V. Kovalenko and W. Heiss, *Nat. Photonics*, 2015, **9**, 444-449.
2. Y. C. Kim, K. H. Kim, D. Y. Son, D. N. Jeong, J. Y. Seo, Y. S. Choi, I. T. Han, S. Y. Lee and N. G. Park, *Nature*, 2017, **550**, 87-91.
3. H. Wei, Y. Fang, P. Mulligan, W. Chuirazzi, H.-H. Fang, C. Wang, B. R. Ecker, Y. Gao, M. A. Loi, L. Cao and J. Huang, *Nat. Photonics*, 2016, **10**, 333-339.
4. W. Pan, H. Wu, J. Luo, Z. Deng, C. Ge, C. Chen, X. Jiang, W.-J. Yin, G. Niu, L. Zhu, L. Yin, Y. Zhou, Q. Xie, X. Ke, M. Sui and J. Tang, *Nat. Photonics*, 2017, **11**, 726-732.
5. X. Hu, X. Zhang, L. Liang, J. Bao, S. Li, W. Yang and Y. Xie, *Adv. Funct. Mater.*, 2014, **24**, 7373-7380.
6. T. J. Octon, V. K. Nagareddy, S. Russo, M. F. Craciun and C. D. Wright, *Adv. Funct. Mater.*, 2016, **4**, 1750-1754.
7. H. Huang, J. Wang, W. Hu, L. Liao, P. Wang, X. Wang, F. Gong, Y. Chen, G. Wu and W. Luo, *Nanotechnology*, 2016, **27**, 445201.
8. L. Xie, L. Guo, W. Yu, T. Kang, R. K. Zheng and K. Zhang, *Nanotechnology*, 2018, **29**, 464002.
9. L. Ye, H. Li, Z. Chen and J. Xu, *ACS Photonics*, 2016, **3**, 692-699.
10. Z. Zheng, T. Zhang, J. Yao, Y. Zhang, J. Xu and G. Yang, *Nanotechnology*, 2016, **27**, 225501.
11. Z.-Q. Xu, Y. Zhang, Z. Wang, Y. Shen, W. Huang, X. Xia, W. Yu, Y. Xue, L. Sun, C. Zheng, Y. Lu, L. Liao and Q. Bao, *2D Materials*, 2016, **3**, 041001.
12. O. Lopez-Sanchez, D. Lembke, M. Kayci, A. Radenovic and A. Kis, *Nat. Nanotechnol.*, 2013, **8**, 497-501.
13. A. Abderrahmane, P. J. Ko, T. V. Thu, S. Ishizawa, T. Takamura and A. Sandhu, *Nanotechnology*, 2014, **25**, 365202.
14. Q. Ou, Y. Zhang, Z. Wang, J. A. Yuwono, R. Wang, Z. Dai, W. Li, C. Zheng, Z. Q. Xu, X. Qi, S. Duhm, N. V. Medhekar, H. Zhang and Q. Bao, *Adv. Mater.*, 2018, **30**, 1705792.

15. Q. Liang, Q. Wang, Q. Zhang, J. Wei, S. X. Lim, R. Zhu, J. Hu, W. Wei, C. Lee, C. Sow, W. Zhang and A. T. S. Wee, *Adv. Mater.*, 2019, **31**, 1807609.
16. C. H. Liu, Y. C. Chang, T. B. Norris and Z. Zhong, *Nat. Nanotechnol*, 2014, **9**, 273-278.
17. M. Buscema, D. J. Groenendijk, S. I. Blanter, G. A. Steele, H. S. Van Der Zant and A. Castellanos-Gomez, *Nano lett.*, 2014, **14**, 3347-3352.
18. Q. Guo, A. Pospischil, M. Bhuiyan, H. Jiang, H. Tian, D. Farmer, B. Deng, C. Li, S.-J. Han and H. Wang, *Nano lett.*, 2016, **16**, 4648-4655.
19. J. Yin, Z. Tan, H. Hong, J. Wu, H. Yuan, Y. Liu, C. Chen, C. Tan, F. Yao, T. Li, Y. Chen, Z. Liu, K. Liu and H. Peng, *Nat. Commun.*, 2018, **9**, 3311.

